Comparing regional breast density using Full-Field Digital Mammograms and Magnetic Resonance Imaging: A preliminary study.

Eloy García[a], Arnau Oliver[a], Yago Diez[a], Oliver Diaz[a], Joachim Georgii[b], Albert Gubern-Mérida[c], Joan Martí[a], and Robert Martí[a]

[a] Computer Vision and Robotics Institute, University of Girona, Spain
[b] Institute of Medical Imaging Fraunhofer MEVIS, Bremen, Germany
[c] Radboud University Medical Center, Nijmegen , The Netherlands
{egarcia,aoliver,yago,oliverdiaz,joanm, marly}@eia.udg.edu;
Joachim.Georgii@mevis.fraunhofer.de;
albert.gubernmerida@radboudumc.nl

Abstract. Breast density is well established as an important risk factor for the development of breast cancer. Therefore, its objective estimation has been the focus of research in the past decades. In addition to global volumetric measures, the local distribution and patterns of this density are currently being investigated to determine whether they can provide complementary information for risk assessment. This paper proposes a framework to evaluate the correlation between local spatial distribution of dense tissue in full-field digital mammograms (FFDM) using a density estimation software (Volpara^{TM}) and magnetic resonance imaging (MRI). Initial results with 51 patients (204 images) showed a significant correlation using several local measures, the largest being 0.81. This indicates that local density patterns estimated in FFDM correlate well with those in MRI. However, pixelwise measures failed to yield the same degree of correlation. This may indicate that the areas where tissue densities are located in both approaches are comparable, but small variations in pixelwise tissue distribution between both approaches exist.

1 Introduction

Full-field digital mammography (FFDM) and magnetic resonance imaging (MRI) are imaging modalities used for the early detection and diagnosis of breast diseases in women. Mammography is an optical process in which the breast is exposed to an X-ray beam to obtain an image of the internal tissue distribution. The relative prevalence of fibroglandular and fat tissues in the breast is inferred from the image pattern of brightness. Fibroglandular has larger X-ray attenuation coefficient than fat tissue and, therefore, appears brighter on mammograms. On the other hand, breast MRI uses a powerful magnetic field and pulses of radio waves to compute detailed images of the internal structure based on the amount of water each tissue contains. Since fibroglandular and fat tissues have different water concentration they can be differentiated in the MRI volume.

Although the physics underlying each modality is different, recent works have demonstrated a high correlation when computing total and percentage dense volume of the same patient using both modalities [2, 6, 12, 13]. In these works, an automated volumetric measurement of the density in FFDM is obtained using a commercial tool (Cumulus V, Quantra^{TM}, Volpara^{TM}), while the density in MRI is segmented using some common segmentation algorithm (i.e. non-commercial tools). Although a high volumetric correlation provides valuable insight into the total amount of dense tissue present in the breast, this does not imply that tissue distribution within the breast is the same. Consequently, new approaches aim at providing local *density maps* where not only the total but also a measure of pixel-wise amount of glandular tissue present in each pixel is provided. This kind of localised density information is rapidly gaining importance due to its diagnostic potential as, for example, a breast cancer risk biomarker [8].

In this paper, we want to go one step further and compare the spatial distribution of glandular tissue using information from both FFDM and MRI modalities. For this purpose, we use the Volpara^{TM} density map to estimate for each pixel of the mammogram the amount of dense tissue traversed by the X-rays converging in that pixel. On the other hand, from the MRI of the patient, we construct a patient-based density map using the projection of a biomechanical compressed model of the breast [3, 7, 9]. Afterwards, evaluation of the similarity is performed using global and local metrics. The rest of this document is organised as follows: Section 2 presents the methods used to compute the breast density maps from FFDM and MRI. Section 3 presents the experiments carried out and discusses the results obtained. The paper finishes with the conclusions.

2 Methodology

2.1 Generating the density map from FFDM

To compute the spatial distribution of breast glandular tissue from mammograms, we used the commercial software Volpara^{TM}. The basis of Volpara software can be found in the work of Highnam et al. [4]. The starting point is to find an area within the mammogram which is entirely adipose (fatty) tissue. This area (P_{fat}) is used as a reference level to compute the thickness of glandular tissue (h_d) at each pixel (x, y) of the mammogram using the following equation:

$$h_d(x, y) = \frac{ln(P(x, y)/P_{fat})}{\mu_{fat} - \mu_{dense}}, \tag{1}$$

where $P(x, y)$ corresponds to the grey level at pixel (x, y), which is proportional to the X-ray energy absorbed at the receptor. The values in the denominator (μ_{fat}, μ_{dense}) represent the effective X-ray linear attenuation coefficients for fat and glandular (dense) tissue respectively at the particular energy spectrum and recorded breast thickness. Integrating the $h_d(x, y)$ values over the entire mammogram, Volpara^{TM} computes the volume of glandular tissue. However, in our case, we will use the information provided by Volpara^{TM} without this final integration. We call it as the FFDM local density map ($D_{FFDM}(x, y)$).

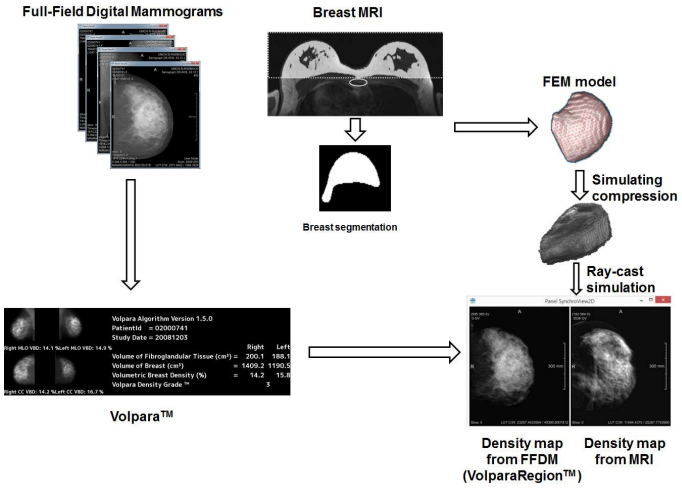

Fig. 1. Scheme of the process to generate and compare density maps.

2.2 Generating the density map from MRI

In order to generate a density map from breast MRI comparable with the one provided by Volpara^{TM}, the acquisition conditions observed in mammography have to be reproduced. Figure 1 illustrates the proposed framework to generate density maps from breast MRI ($D_{MRI}(x, y)$) and compare them with Volpara^{TM}.

Firstly, the 3D breast MR volume is segmented from the background using a methodology similar to the one presented by Gubern-Mérida et al. [2]. Subsequently, internal tissues are further segmented using an intensity-based Expectation-Maximisation algorithm that allows obtaining a 3D density probability map of the whole MRI volume. In other words, each voxel contains its probability of belonging to the glandular tissue class.

The biomechanical breast model is simulated using a similar procedure as the one proposed by Mertzanidou et al. [7]. The breast mask is down-sampled to isotropic voxels of 4 mm length, generating a volumetric tetrahedral mesh with a high number of elements (approx. 100,000). During the compression process, only a single material is considered for the breast model (glandular labels will be added after the breast model is compressed). These approximations will avoid convergence problems of the finite element solver [7, 9]. With this simplification, the stress-strain relationship is approximated by a nearly incompressible, isotropic, and hyperelastic neo-Hookean model [5], which uses a Young's modulus equal to 4 KPa. The compression paddle was simulated using a frictionless contact model, and the nodes belonging to the breast-body interface are allowed to slide along its surface [3]. The necessary information to reproduce the mammographic compression (breast thickness, view angle, source-to-detector distance, etc...) is extracted from the DICOM header of the corresponding mammogram.

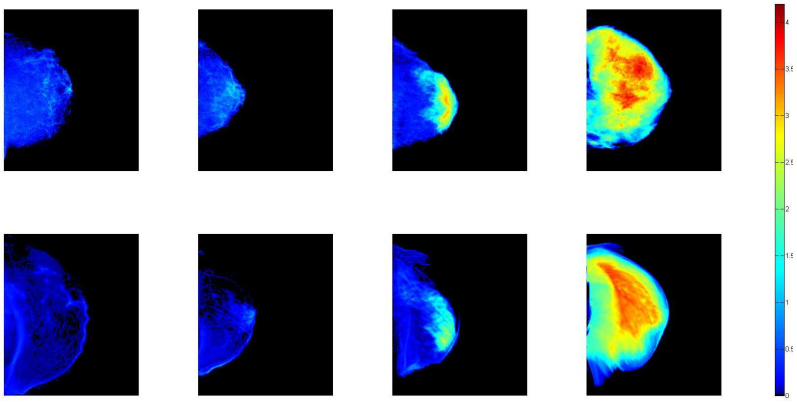

Fig. 2. Four different examples of density maps obtained from FFDM (upper row) and MRI (bottom row). The breasts are ordered with increasing density from left to right. The thickness scale is shown in centimeters.

In FFDM, once the breast is compressed, the mammogram is generated from the projection of a cone beam of X-ray photons traversing the breast. Here, a ray-casting algorithm [11] is used, in conjunction with the compressed breast model, to simulate the mammographic geometry and compute the amount of glandular tissue traversed by each X-ray photon at different locations of the receptor. The resolution of this density map ($D_{MRI}(x, y)$) depends on the sampling distance used in the ray-casting. The more points used, the higher the resolution will be. However, the computational time will also be more expensive. In our experiments, 2D $D_{MRI}(x, y)$ of resolution 0.2 mm were generated. Examples of the density maps obtained with this approach along with the ones obtained from the mammograms are shown in Figure 2.

2.3 Image registration

In order to provide a fair comparison of the two density maps generated ($D_{FFDM}(x, y)$ and $D_{MRI}(x, y)$) we need to align both images as much as possible. To achieve this, we use two registration steps. Firstly, a 3D/2D registration step is performed, where the 3D compressed biomechanical breast model is slid in the direction parallel to the plane containing the mammography. The optimisation process consists in finding the minimum least squares distance between the boundary of the 2D projection of the breast model and the boundary of the original mammogram. Once the optimal position of the compressed breast model is found, $D_{FFDM}(x, y)$ is calculated as previously explained.

Secondly, a 2D/2D registration between $D_{FFDM}(x, y)$ and $D_{MRI}(x, y)$ is used to account for small, localised deformations produced by simplification assumptions and possible interpolation errors. For this step we tested commonly used registration algorithms such as rigid, affine, B-Splines, and Demons [1].

3 Results

The dataset used contained 51 T1 MR images and 204 CC and MLO mammograms that were randomly sampled from a larger high-risk women screening dataset acquired retrospectively at the Radboud University Medical Centre. The 51 patients were aged 24 to 77 (mean: 45.96 ± 12.56). Two different MRI scanners were used: 1.5 and 3 Tesla Siemens scanner (Magnetom Vision, Magnetom Avanto and Magnetom Trio) with dedicated breast coil (CP Breast Array, Siemens, Erlangen). The time between the acquisition of the MRI and the mammographic images was at most 2 months (being performed within two weeks of each other for most cases).

Evaluating the degree of similarity between density maps obtained from FFDM and MRI is a challenging problem. It joins the difficulty of evaluating the quality of registration [1, 10] with the measurement and interpretation of the density values. We tackled this problem using measures of two different types:

- Global measures. The goal of these measures is to provide a single value per density map pair indicating their degree of similarity. Specifically, we used mutual information (MI), the Dice coefficient of dense tissue overlap, and texture measures. MI provides an indicator on the degree of success of the registration algorithms used. The evaluation of the dense tissue overlap aims at singling out the contributions of each tissue type to the quality of registration. Finally, texture comparison targets local properties of the pixels in both density maps (although still one single value is produced per image).
- Local measures. Ideally, a pixel-to-pixel comparison of both density maps should be used to assess how similar they are. However, this results in an underestimation of the similarity of both maps due to small misalignments of the breast model. Therefore, we consider computing the similarity by extracting first order statistics in small windows instead of pixels.

Before focusing in local density, we compared the global volumetric breast density estimation computed by Volpara^{TM} and our probabilistic MRI segmentation. The Pearson's correlation of the global dense tissue volume computed by both methods was 0.85, the same achieved in Gubern-Mérida et al. [2]. Similarly to that work, discrepancies are found in some examples due to the presence of skin voxels not correctly segmented before the tissue segmentation or problems with the bias field correction approach.

3.1 Global measures

Figure 3 shows the MI values obtained when registering 2D/2D density maps. A large value indicates higher agreement between them. The first boxplot corresponds to the MI evaluated before this step. The figure shows that rigid, affine, and B-spline registration methods manage to improve the values, although only B-splines achieves a statistically significant improvement (difference of means test, $\alpha = 0.05$).

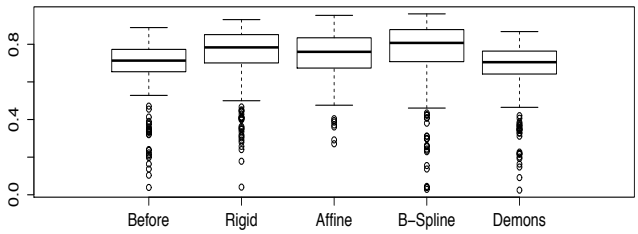

Fig. 3. Mutual information comparison containing the 204 comparisons between the density maps obtained using FFDM and MRI of the same patient. The more similar the images, the larger the mutual information (y-axis).

Table 1. Dice coefficients computed between density maps of the same patient.

	Before	Rigid	Affine	B-Spline	Demons
Dice's coef.	0.67 ± 0.17	0.74 ± 0.17	0.73 ± 0.13	0.75 ± 0.20	0.67 ± 0.16

Table 1 shows the Dice coefficient overlap obtained when thresholding the density map at a given density percentage detailed for the used 2D/2D registration algorithm. The high overlap obtained implies that dense areas in both maps are located in a similar region. Regarding the registration algorithms, the same behaviour seen in the MI plot is obtained, where Demons fails to improve the similarity between both density maps.

We finally computed and compared texture measures in both density maps. Texture takes spatial neighbourhoods into account, although we consider it a global measure since a single value is computed per image. Hence, the comparison of the obtained texture values in both density maps allows evaluating their local similarity. Table 2 shows the correlation obtained using four different statistics based on Haralick's co-occurrence matrices computed at a distance of 16 pixels for both density maps. Notice that the energy and homogeneity features in both maps are highly correlated, while contrast and correlation are low. Regarding algorithms, rigid, affine, and B-spline achieve a higher correlation while demons shows a low performance in the correlation feature. These results show that dense areas are spatially correlated (as shown by the energy feature) but they present differences in the amount of density of the neighbourhood (as indicated by the contrast feature). These differences could be explained by misalignments due to misregistration. The images shown in Figure 2 reflect this situation.

3.2 Local measures

The last evaluation measure used relates local measurements in the density maps obtained by Volpara^{TM} and MRI. Experiments show that pixel-wise comparison fails because small misalignments of the breast model across the whole process

Table 2. Pearson's correlation coefficients of texture measures computed between density maps of the same patient.

	Before	Rigid	Affine	B-Spline	Demons
Energy	0.70	0.73	0.73	0.72	0.69
Contrast	0.30	0.29	0.18	0.28	0.27
Homogeneity	0.64	0.71	0.73	0.73	0.63
Correlation	0.32	0.29	0.43	0.20	0.32

Table 3. Pearson's correlation coefficients of intensity mean and standard deviation computed in blocks of 16×16 pixels between density maps.

	Before	Rigid	Affine	B-Spline	Demons
Mean	0.54	0.64	0.70	0.81	0.57
Std	0.05	0.10	0.11	0.14	0.09

can result in small, localised discrepancies. These differences do not faithfully reflect the similarity of the density maps. To overcome this issue, we divided the breast density maps into small regions of 16×16 pixels ($\approx 5 \times 5$ mm) and computed pixel intensity mean and standard deviation of those blocks. Afterwards, we calculated the correlation of those statistics before and after registration.

Table 3 summarises the local measures obtained before and after the registration step. Discrepancies in the comparison stem from two main sources. On the one hand, observed differences might result from suboptimal registration. Table 3 shows how B-spline is the best registration method, achieving a correlation value of 0.81 between the dense tissue thickness computed from FFDM and MRI when evaluating the mean glandular thickness of each 16×16 pixels block. Conversely, other methods fail to show the same correlation for the exact set of images. On the other hand, discrepancies could also be due to actual small differences in tissue distribution. As also stated in the analysis of the texture features, it seems that the areas where tissue densities are located are comparable, but micro-density is computed differently in both approaches.

4 Conclusions

In this paper, we have compared the regional breast density estimation obtained using FFDM and MRI. Specifically, we have used the Volpara^{TM} software for obtaining the FFDM density map and a patient-specific biomechanical model for obtaining the MRI density map. Our results, evaluated in a large dataset containing 204 FFDM and 51 MRI, showed that both density maps present high similarity in terms of global image metrics as well as a large degree of overlap of the areas containing dense tissue. We have also seen that pixel-wise measures provide suboptimal results for areas where the tissue is denser. This happens because of small variations within the dense tissue due to registration imperfections. In order to prove this, we explored what happened in local areas in

terms of small windows. A high degree of correlation between FFDM and MRI measurements was subsequently observed. Further work will focus on improving the MRI 3D/2D registration process by allowing for the variation of more parameters. This might result in a slower but more accurate approach.

Acknowledgement

The research leading to these results has received funding from the European Union's Programme FP7 under Grant Agreement No. 306088 and by the Spanish R+D+I grant TIN2012-37171-C02-01. E. García holds the FPI scholarship BES-2013-065314.

References

1. Diez, Y., Oliver, A., Lladó, X., et al.: Revisiting intensity-based image registration appplied to mammography. IEEE Trans Inf Technol Biomed 15(5), 716–725 (2011)
2. Gubern-Mérida, A., Kallenberg, M., Platel, B., et al.: Volumetric breast density estimation from full-field digital mammograms: A validation study. Plos One p. e85952 (2014)
3. Han, L., Hipwell, J., Tanner, C., et al.: Development of patient-specific biomechanical models for predicting large breast deformation. Phys Med Biol 57(2), 455–472 (2012)
4. Highnam, R., Brady, M., Yaffe, M.J., et al.: Robust breast composition measurement - Volpara^{TM}. In: Int W Digital Mammography. Lect Notes Comput Sc, vol. 6136, pp. 342–349 (2010)
5. Hopp, T., Ruitter, N.: 2D/3D registration for localization of mammographycally depicted lesions in breast MRI. In: Int W Digital Mammography. Lect Notes Comput Sc, vol. 7361, pp. 627–634 (2012)
6. Lu, L.J.W., Nishino, T.K., Johnson Jr., R.F., et al.: Comparison of breast tissue measurements using magnetic resonance imaging, digital mammography and a mathematical algorithm. Phys Med Biol 57(21), 6903–6927 (2012)
7. Mertzanidou, T., Hipwell, J., Johnsen, S., et al.: MRI to X-ray mammography intensity-based registration with simultaneous optimisation of pose and biomechanical transformation parameters. Med Image Anal 18(4), 674–683 (2014)
8. Otsuka, M., Harkness, E., Chen, X., et al.: Local breast density at lesion sites in diagnostic and previous screening mammograms. Breast Cancer Res 16(Suppl 1), O4 (2014)
9. del Palomar, A., Calvo, B., Herrero, J., et al.: A finite element model to accurately predict real deformations of the breast. Med Eng Phys 30(9), 1089–1097 (2008)
10. Rohlfing, T.: Image similarity and tissue overlaps as surrogates for image registration accuracy: Widely used but unreliable. IEEE Trans Med Imag 31(2), 153–163 (2012)
11. Roth, S.: Ray casting for modeling solids. Comput Graph Image Process 18(2), 109–144 (1982)
12. Tagliafico, A., Tagliafico, G., Astengo, D., et al.: Comparative estimation of percentage breast tissue density for digital mammography, digital breast tomosynthesis, and magnetic resonance imaging. Breast Cancer Res Treat 138(1), 311–317 (2013)
13. Wang, J., Azziz, A., Fan, B., et al.: Agreement of mammographic measures of volumetric breast density to MRI. Plos One 8(12), e81653 (2012)